

Reduction of impurity confinement time by combined heating of LHW and ECRH in EAST

Zong Xu(许棕), Zhen-Wei Wu(吴振伟), Ling Zhang(张凌), Yue-Heng Huang(黄跃恒), Wei Gao(高伟), Yun-Xin Cheng(程云鑫), Xiao-Dong Lin(林晓东), Xiang Gao(高翔), Ying-Jie Chen(陈颖杰), Lei Li(黎嫘), Yin-Xian Jie(揭银先), Qing Zang(臧庆), Hai-Qing Liu(刘海庆), and EAST team

Citation: Chin. Phys. B, 2021, 30 (**7**): 075202. DOI: 10.1088/1674-1056/abe1a6
Journal homepage: http://cpb.iphy.ac.cn; http://iopscience.iop.org/cpb

What follows is a list of articles you may be interested in

Hardening effect of multi-energy $^{W2+}$-ion irradiation on tungsten–potassium alloy

Yang-Yi-Peng Song(宋阳一鹏), Wen-Bin Qiu(邱文彬), Long-Qing Chen(陈龙庆), Xiao-Liang Yang(杨晓亮), Hao Deng(邓浩), Chang-Song Liu(刘长松), Kun Zhang(张坤)†, and Jun Tang(唐军)‡

Chin. Phys. B, 2020, 29 (**10**): 105202. DOI: 10.1088/1674-1056/ab9c09

Determination of activation energy of ion-implanted deuterium release from W-Y_2O_3

Xue-Feng Wang(王雪峰), Ji-Liang Wu(吴吉良), Qiang Li(李强), Rui-Zhu Yang(杨蕊竹), Zhan-Lei Wang(王占雷), Chang-An Chen(陈长安), Chun-Rong Feng(冯春蓉), Yong-Chu Rao(饶咏初), Xiao-Hong Chen(谌晓洪), Xiao-Qiu Ye(叶小球)

Chin. Phys. B, 2020, 29 (**6**): 065205. DOI: 10.1088/1674-1056/ab8204

Estimation of tungsten production from the upper divertor in EAST during edge localized modes

Jing Ou(欧靖), Nong Xiang(项农), Zong-Zheng Men(门宗政), Ling Zhang(张凌), Ji-Chan Xu(许吉禅), Wei Gao(高伟)

Chin. Phys. B, 2019, 28 (**12**): 125201. DOI: 10.1088/1674-1056/ab5279

Nucleation and growth of helium bubble at (110) twist grain boundaries in tungsten studied by molecular dynamics

Fang-Biao Li(李芳镖), Guang Ran(冉广), Ning Gao(高宁), Shang-Quan Zhao(赵尚泉), Ning Li(李宁)

Chin. Phys. B, 2019, 28 (**8**): 085203. DOI: 10.1088/1674-1056/28/8/085203

Numerical study of influence of *J*×*B* force on melt layer under conditions relevant to ITER ELMs

Yan Huang(黄艳), Ji-Zhong Sun(孙继忠), Juan Cai(蔡娟), Zhen-Yue Sun(孙振月), Chao-Feng Sang(桑超峰), De-Zhen Wang(王德真)

Chin. Phys. B, 2019, 28 (**4**): 045201. DOI: 10.1088/1674-1056/28/4/045201

Reduction of impurity confinement time by combined heating of LHW and ECRH in EAST*

Zong Xu(许棕)[1,2], Zhen-Wei Wu(吴振伟)[3,†], Ling Zhang(张凌)[3,‡], Yue-Heng Huang(黄跃恒)[1,2], Wei Gao(高伟)[3], Yun-Xin Cheng(程云鑫)[3,4], Xiao-Dong Lin(林晓东)[1,2], Xiang Gao(高翔)[1,2,3], Ying-Jie Chen(陈颖杰)[3], Lei Li(黎嫘)[3,4], Yin-Xian Jie(揭银先)[1,2,3], Qing Zang(臧庆)[1,2,3], Hai-Qing Liu(刘海庆)[3], and EAST team[3]

[1] *Advanced Energy Research Center, Shenzhen University, Shenzhen* 518060, *China*
[2] *Key Laboratory of Optoelectronic Devices and Systems of Ministry of Education and Guangdong Province, College of Optoelectronic Engineering, Shenzhen University, Shenzhen* 518060, *China*
[3] *Institute of Plasma Physics, Chinese Academy of Sciences, Hefei* 230031, *China*
[4] *University of Science & Technology of China, Hefei* 230031, *China*

(Received 31 October 2020; revised manuscript received 27 January 2021; accepted manuscript online 1 February 2021)

The core impurity confinement properties are experimentally investigated in the Experimental Advanced Superconducting Tokamak (EAST) plasma heated by lower hybrid wave (LHW) and electron cyclotron resonance heating (ECRH) (LHW+ECRH). It is shown that the impurity confinement time (τ_{imp}) in the L-mode plasma jointly heated by LHW and ECRH is weakly dependent on electron density but strongly dependent on the heating power, thus it is shorter than that in LHW-only heated L-mode plasma with the similar plasma parameters. The combined heating of LHW and ECRH can reduce the collisionality and indicates a more effective heating method for core τ_{imp} reduction and normalized poloidal beta (β_P) improvement. It should be emphasized that in this high β_P operation window the small ELM regime can be accessed, and an L-mode level τ_{imp} (40 ms–80 ms) and high β_N (~ 1.7) can be obtained simultaneously. It means that this typical small ELMy H-mode regime has an advantage in avoiding the serious tungsten accumulation, and will be competitive in future long-pulse steady-state and high-performance operation with high-Z material plasma-facing components.

Keywords: LHW and ECRH heating, impurity confinement time, tungsten, small ELMs regime, EAST

PACS: 52.25.Fi, 52.35.Ra, 52.25.Vy, 52.20.Hv **DOI:** 10.1088/1674-1056/abe1a6

1. Introduction

The high-Z impurities' transport in plasma plays a significant role in present tokamak devices and future fusion devices such as International Thermonuclear Experimental Reactor (ITER) and China Fusion Engineering Test Reactor (CFETR). The high-Z impurities in the plasma core can bring about two deleterious effects: one is strong radiation causing the central power loss,[1] the other is radiative cooling probably leading to plasma disruption.[2] High-Z impurities in the central plasma therefore need to be controlled, especially in a machine with tungsten (W, $Z = 74$) divertor plates, where physical sputtering at the striking points can inject tungsten into the main plasma.[3]

Previous research results in terms of experiments and simulations demonstrated that the impurity accumulation can be suppressed by intense central electrons heating.[4–7] Widely used in DIII-D,[8,9] ASDEX-U,[10] TCV,[11] *etc*., the on-axis ECRH can provide a more peaked electron temperature in plasma core so as to avoid the impurity accumulation. The LHW heating utilized on Tore Supra[12] and EAST[13,14] also shows an apparent reduction of core impurity confinement, due to the fact that LHW can heat central electron and generate turbulent transport. The study of the core impurity confinement properties in LHW and ECRH heated plasmas was inspired by the intense central electron heating.[15–17] Furthermore, in EAST, it is observed that the combined heating of LHW and ECRH can alleviate and avoid the effect of the sawtooth oscillation on the impurity transport.[18–20] The results regarding this combined heating for improving the core impurity confinement will be beneficial to the EAST long-pulse steady-state and high-performance operation with tungsten divertor.

The rest of the paper is structured as follows. In Section 2 described are the radio-frequency (RF) heating systems and the relevant diagnostics in EAST. In Section 3 provided are the experimental studies of the metallic impurity confinement properties in LHW and ECRH heated discharges. Finally in Section 4 summary and discussion are presented.

*Project supported by the National Key Research and Development Program of China (Grant Nos. 2018YFE031110 and 2017YFE0301205), the National Natural Science Foundation of China (Grant Nos. 11905146, 11775269, and 11805113), the Users with Excellence Program of Hefei Science Center, Chinese Academy of Sciences (Grant No. 2019HSC-UE014), and the Fund from the Shenzhen Clean Energy Research Institute, China.

†Corresponding author. E-mail: zwwu@ipp.ac.cn
‡Corresponding author. E-mail: zhangling@ipp.ac.cn

© 2021 Chinese Physical Society and IOP Publishing Ltd

2. Experimental setup

This work was carried out on the full superconducting EAST tokamak, in which the vacuum chamber has a major radius R of 1.85 m and minor radius a of 0.45 m, the plasma cross-section elongation ratio k from 1.2 to 2, maximum plasma current I_P is 1 MA, maximum designed center toroidal field strength B_t is 3.5 T, and there are an advanced and flexible divertor configuration. The auxiliary heating systems have been successively developed since the first plasma was obtained in the 2006 campaign of EAST.[21] The RF heating methods, routinely used in EAST long-pulse and steady-state operated discharges, include two sets of LHW heating systems (a maximum power of 4 MW at 2.45 GHz, and a maximum power of 6 MW at 4.6 GHz),[22,23] two sets of ion cyclotron resonance frequency (ICRF) heating systems with a maximum total power of 12 MW in a frequency range of 25 MHz–70 MHz,[24] and two sets of ECRH systems with a maximum total heating power of 1 MW at 140 GHz.[25] Moreover, EAST has upgraded the plasma facing components (PFCs) to optimize the capacity of the heat load. The present main PFCs materials in EAST vacuum are W/Cu mono-blocks with active water-cooling for the upper divertor, molybdenum (Mo, $Z = 42$) plates for the first wall, and SiC-coated graphite tiles for the lower divertor. In addition, there are metallic materials mounted for some special purposes, such as tungsten tiles for one of the guard limiters of LHW, copper (Cu, $Z = 29$) for the RF antenna panels (including ICRF, LHW, and ECRH), and stainless steel (Fe, $Z = 26$) for the dedicated ICRF antenna. The high-Z metallic impurities in these components can be sputtered into the main plasma through the process of plasma surface interaction (PSI), degrading the plasma performance.

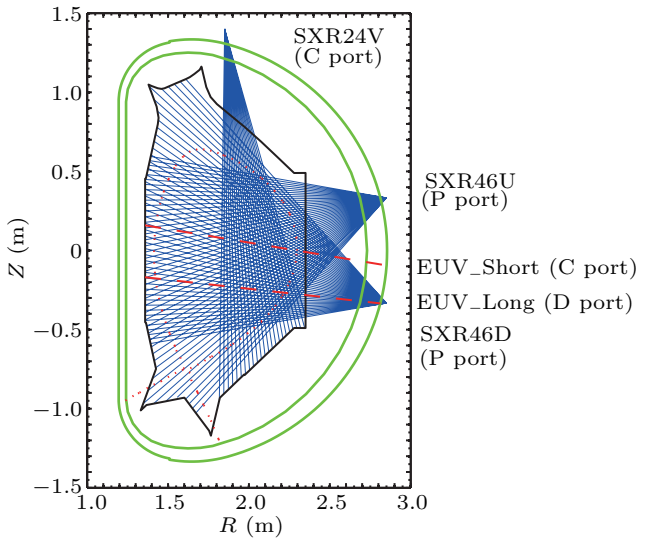


Fig. 1. Sight field of soft x-ray imaging system (the blue lines) and viewing chords of two EUV spectrometers: EUV_Short (dashed black line) and EUV_Long (red lines) in EAST cross section.

Figure 1 shows the field of view of the soft x-ray imaging system,[26] which can cover the whole plasma poloidal cross-section by using 116 lines of sight (LOS). The viewing chords of two EUV spectrometers (EUV_Short and EUV_Long) are also exhibited in this figure. The EUV_Short and EUV_Long[27] work in a wavelength range of 20 Å–50 Å and 20 Å–500 Å, respectively, and both have good temporal and spectral resolutions for measuring the chord-integrated line emission intensity emitted from impurity ions. These diagnostic tools enable the effective investigating of the core impurity behavior inside $r/a \sim 0.4$. Other needed diagnostic tools include the Thomson scattering system for measuring the electron density and temperature profile, the polarimeter-intferometer (POINT) for measuring the electron density profile, and the far-infrared (FIR) hydrogen cyanide (HCN) laser interferometer for measuring the lineaveraged electron density.

3. Experimental results

The studies of impurity confinement by using LHW and ECRH heating are carried out in L- and H-mode plasma on EAST. In this analysis, the τ_{imp} defined below is used to estimate the efficiency of the heating methods for impurity accumulation control.

3.1. Spontaneous transient perturbations of impurities in EAST

The τ_{imp} is the slowest time constant corresponding to the fundamental eigenfunction and can describe the decay of the final impurity distribution,[28,29] which has been used on many tokamak devices, such as C-mod,[30] TCV,[31] JET,[32] *etc.* Experimentally, the τ_{imp} is often deduced by so-called transient perturbation method (TPM), in which, the decay of transient impurity perturbation induced by the active impurity-producing techniques (such as, laser blow-off, pellets injection and gas puffing) is used for analyzing the impurity transport.[28,29,33]

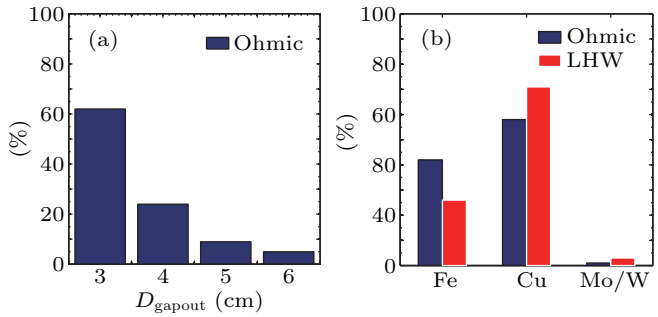


Fig. 2. (a) Probability of transient impurity sputtering events *versus* D_{gapout} (distance of outer gap between limiter and last closed flux surface) in ohmically L-mode discharges (total 509 shots), and (b) probability of species of the sputtered impurities in ohmically (dark blue color) and LHW (red color) heated L-mode discharges (total 1433 shots) respectively.

As there is no active technique for injecting metallic impurities on EAST, the spontaneous transient perturbations of medium and high-Z impurities are chosen for calculating the $\tau_{\rm imp}$. This spontaneous TPM has been successfully used to study the confinement properties of Fe and Cu in LHW-heated sawtooth-free plasma on EAST.[13] Such a spontaneous TPM of metallic impurities always occurs when the distance of outer gap between the limiter and the last closed flux surface ($D_{\rm gapout}$) is relatively small. It is found that more than 80% of transient perturbation events happen when $D_{\rm gapout} < 4$ cm, such as in the ohmic plasma shown in Fig. 2(a). In the L-mode discharge with ohmic and pure-LHW heating, such transient perturbations are caused mainly by iron and copper ions as shown in Fig. 2(b). The transient perturbation of copper ions induced by the 'hotspots' from the LHW antenna panels are confirmed by high-speed CCD camera and EUV spectrometers.[13] However, the transient perturbation caused by molybdenum or tungsten ions is rarely observed because of the high sputtering threshold of molybdenum and tungsten ions. The shots with the perturbations of molybdenum and tungsten ions are mainly due to the dust-dropping or the interaction between the plasma particles and the testing samples.

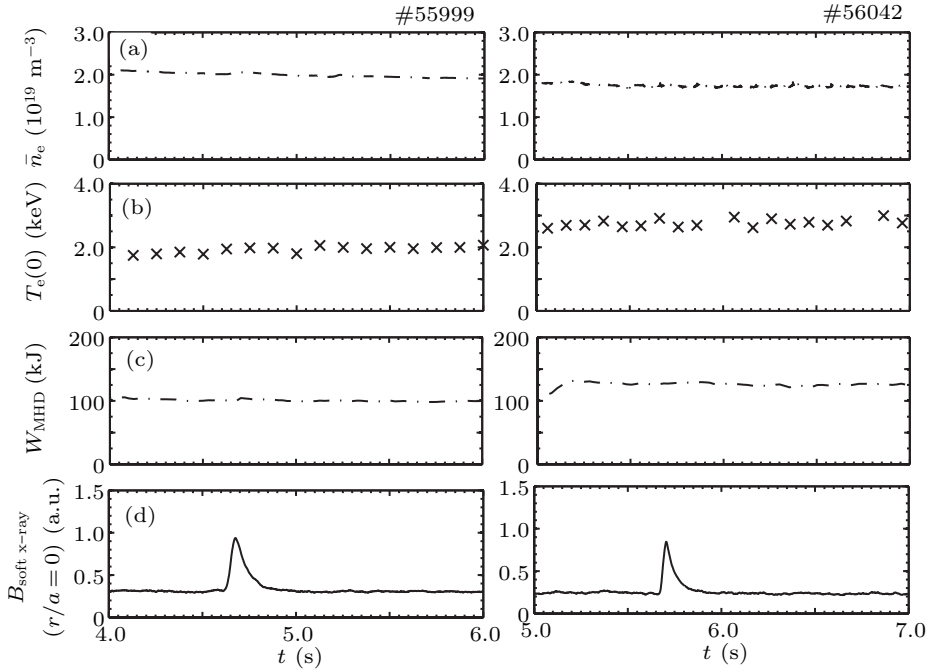


Fig. 3. Time traces of pulses # 55999 and #56042 during 4.0 s–6.0 s and 5.0 s–7.0 s, respectively: (a) line-averaged electron density $\bar{n}_e$, (b) central electron temperature $T_e(0)$, (c) stored energy $W_{\rm MHD}$, and (d) soft x-ray emission from central chord.

The perturbation of impurity can be displayed by soft x-ray emission signals and EUV spectra. Taking shots #55999 (LHW-only) and #56042 (LHW+ECRH) for example, in Fig. 3(d), perturbations are revealed by the spikes on the central soft x-ray signal. The species of the sputtered impurities causing the spikes on the soft x-ray emission signal can be identified by the fast EUV spectrometers. The intensities of the line emissions from intrinsic impurities in shots #55999 and #56042, such as $C_{\rm VI}$ (33.73 Å), $Li_{\rm III}$ (134.99 Å), $Fe_{\rm XXII}$ (117.17 Å), and $Cu_{\rm XXVI}$ (111.186 Å), are given in Fig. 4. It can be seen that the spikes on the intensity of $Fe_{\rm XXII}$ (#55999) and $Cu_{\rm XXVI}$ (#56042) emissions indicate that iron and copper ions penetrate deep into the plasma. Subsequently, the spikes decay nearly exponentially due to the diffusion of iron and copper ions out of the plasma. Therefore, it can be confirmed that the spikes on the soft x-ray signals are caused by iron ions for shot #55999 at 4.62 s and by copper ions for shot #56042 at 5.66 s respectively. The enhancement of intensity of $C_{\rm VI}$ emission during the ECRH heating phase in shot #56042 is due to the thermally overloaded wall protection tiles (graphite tiles embedded on the high field side of the first wall) on the opposite to the ECRH antennas, can be seen in Fig. 4(a).

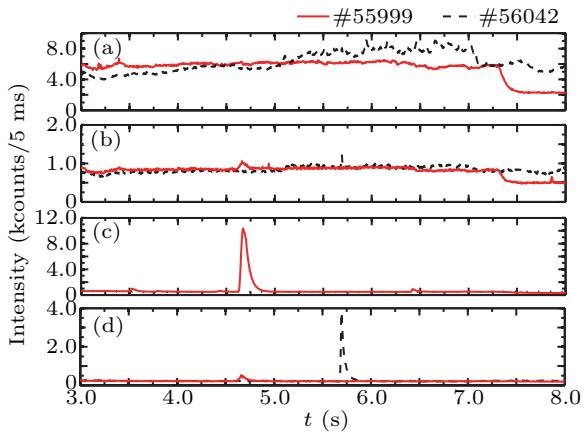


Fig. 4. Time evolutions of intensities of line emissions from intrinsic impurities of shots #55999 (solid red line) and #56042 (dashed black line): (a) $C_{\rm VI}$ 33.73 Å, (b) $Li_{\rm III}$ 134.99 Å, (c) $Fe_{\rm XXII}$ 117.17 Å, and (d) $Cu_{\rm XXVI}$ 111.186 Å.

The response of the plasma parameters to the perturbation of impurities is shown in Fig. 3. Generally, the TPM can be utilized on the central chord of soft x-ray emission signal only in the case that the effect of the impurity perturbation on electron density $\bar{n}_e$ or electron temperature $T_e(0)$ does not exceed 10%,[12,28] as the intensity of soft x-ray emission is determined by $\bar{n}_e$ and $T_e(0)$ ($\propto \bar{n}_e^2 T_e^\gamma$, $\gamma = 2$–5). As clearly seen from Fig. 3, the plasma parameters for each of both shots are not obviously affected by transient perturbation of impurity events.

An exponential function $A\,e^{(-t/\tau_{imp})} + B$ is used to fit the decay phase of the soft x-ray signal. The relative error of the fitted decay time is less than 2% with the 95% confidence interval. It is found that a nearly constant decay time is obtained after the soft x-ray signal has decayed $\sim 20\%$ as shown in Fig. 5(b). Figure 5(c) also shows the decay times of several chords of soft x-ray signal at different locations ($r/a = 0$–0.4). It indicates that the decay time at the location of $r/a = 0$ is larger than at other locations, for the diffusion is lower in the inner plasma which thus governs the τ_{imp}. So, in order to guarantee that the decay phase is determined by the τ_{imp}, the fit must start till the brightness of central chord of soft x-ray emission has decayed about 20%–40% from its peak.

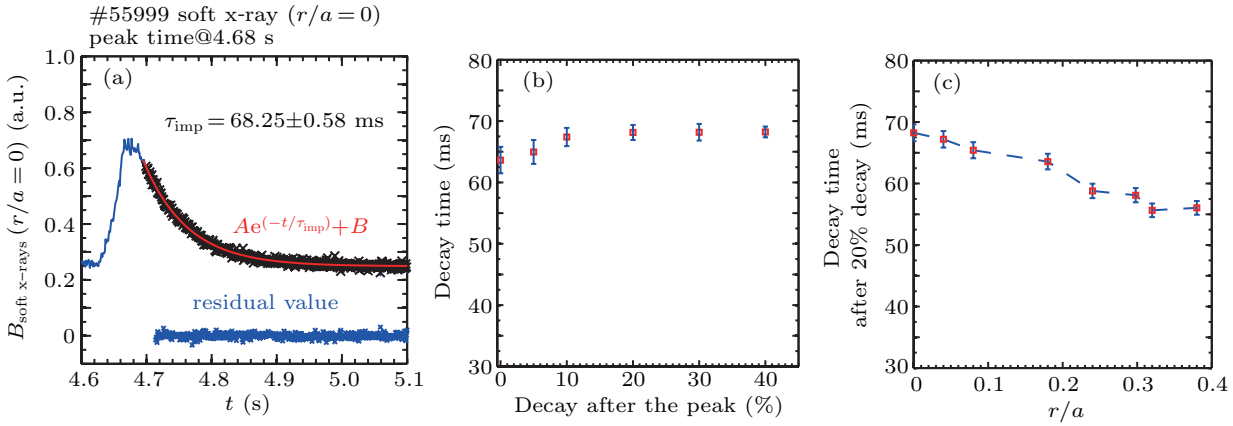


Fig. 5. (a) Reconstruction of soft x-ray signal with function $A\,e^{(-t/\tau_{imp})} + B$ in decay phase of spike (red dashed line), (b) decay time *versus* decay after peak, and (c) decay time calculated by fitting the different chords of soft x-ray signal near locations $r/a = 0$–0.4.

3.2. Comparison between τ_{imp} in L-mode plasma with LHW and LHW+ECRH heating

3.2.1. Dependence of τ_{imp} on electron density and total heating power

The previous investigation shows that the τ_{imp} value increases with $\bar{n}_e^{0.43} P_{total}^{-0.4}$ increasing in ohmically heated L-mode plasma and pure-LHW-heated L-mode plasma in EAST.[13] But the dependence of τ_{imp} on $\bar{n}_e$ and P_{total} (total heating power) is different from that in the plasma with combined heating of LHW and ECRH. The τ_{imp} values *versus* $\bar{n}_e^{0.43}$ in discharges with pure-LHW heating and with combined heating of LHW and ECRH are shown in Fig. 6. The chosen shots are obtained at $I_P = 0.3$ MA–0.5 MA, $\bar{n}_e = 1.5 \times 10^{19}$ m^{-3}–4.0×10^{19} m^{-3}, $B_t = 2.25$ T–2.55 T, and total heating power $P_{total} = 1.3$ MW–1.6 MW, where in the shots with combined heating, the input power of ECRH, $P_{ECRH} = 0.2$ MW–0.5 MW. In Fig. 6, the red and black triangles indicate the shots with pure-LHW heating and combined heating of LHW and ECRH respectively. In pure-LHW heated L-mode discharges, the τ_{imp} values increase with $\bar{n}_e^{0.43}$ increasing obviously. Noticeably, as the electron density increases, the absorbed power of LHW will decrease in central plasma which causes central electrons to be weakly heated.[34] In this case, the higher the electron density, lower central electron temperature can make impurity diffusivity in core plasma decrease due to the collisional transport.[35] But for the shots with combined heating, the τ_{imp} values are lower than for the shots with pure LHW heating and just slightly increase with $\bar{n}_e^{0.43}$. Even for the shots with higher electron density, the on-axis ECRH can heat the central plasma as well as improve the LHW heating capability due to the increased background electron temperature[34] or the synergy effect.[16,17,36] It can be inferred that the τ_{imp} is weakly dependent on $\bar{n}_e$ but strongly dependent on P_{total} in the shots with combined heating of LHW and ECRH.

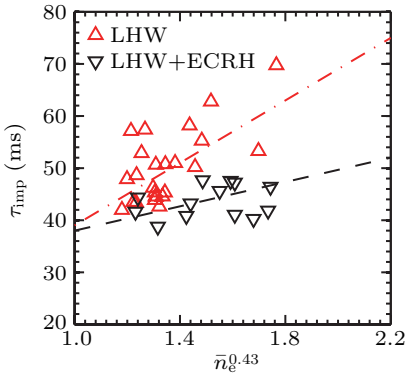


Fig. 6. The τ_{imp} values *versus* $\bar{n}_e^{0.43}$ in discharges with pure-LHW heating (red triangles) and with combined heating of LHW and ECRH (black triangles).

The τ_{imp} values *versus* $P_{total}^{-0.4}$ in the discharges with combined heating of LHW and ECRH are shown in Fig. 7. The chosen shots are obtained at $\bar{n}_e = 1.5 \times 10^{19}$ m^{-3}–$2.3 \times$

10^{19} m^{-3} and $P_{\rm total} = 0.5$ MW–2.5 MW (where $P_{\rm ECRH} =$ 0.2 MW–0.5 MW). As clearly shown in Fig. 7, the $\tau_{\rm imp}$ values do not increase monotonically with $P_{\rm total}^{-0.4}$ increasing in the discharges with combined heating. When the $P_{\rm total}$ is higher ($P_{\rm total}^{-0.4} < 1.2$), the $\tau_{\rm imp}$ value increases with $P_{\rm total}^{-0.4}$ increasing. But when the $P_{\rm total}$ is lower and ECRH becomes the dominant heating ($P_{\rm ECRH}/P_{\rm total} \geq 0.4$), the $\tau_{\rm imp}$ value will deviate from the tendency of $P_{\rm total}^{-0.4}$ and keep a lower level due to the peaked central electron temperature provided by ECRH as shown in square box of Fig. 7. The results regarding the dependence of $\tau_{\rm imp}$ value on $\bar{n}_{\rm e}^{0.43} P_{\rm total}^{-0.4}$ indicate that the $\tau_{\rm imp}$ value in the L-mode plasma heated by combined heating of LHW and ECRH cannot be well predicted by EAST's scaling law[13]

$$\tau_{\rm EAST}\,({\rm ms}) = 42 I_{\rm P}^{0.32} B_{\rm t}^{0.2} \bar{n}_{\rm e}^{0.43} P_{\rm total}^{-0.4}, \quad (1)$$

where $I_{\rm P}$ is in unit of MA, $B_{\rm t}$ is in unit of T, $\bar{n}_{\rm e}$ is in unit of 10^{19} m^{-3}, and $P_{\rm total}$ is in unit of MW. This combined heating method allows a higher electron density operation and can avoid the serious impurity accumulation, which is beneficial to high normalized poloidal beta ($\beta_{\rm P}$) plasma obtainment.[37]

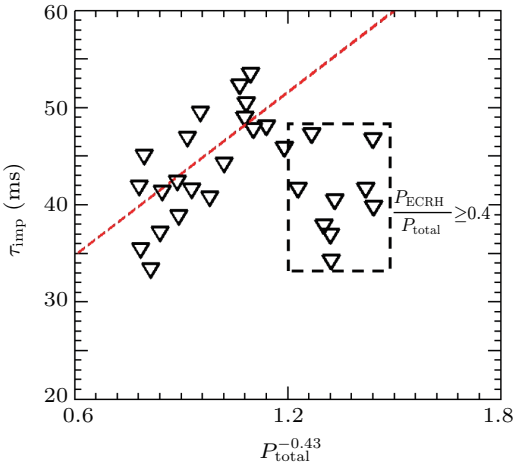


Fig. 7. Measured $\tau_{\rm imp}$ values *versus* $P_{\rm total}^{-0.4}$ in discharges with combined heating of LHW and ECRH.

3.2.2. Dependence of $\tau_{\rm imp}$ on effective collisionality

Figure 8 shows the measured $\tau_{\rm imp}$ values and integrated power of turbulence (at wave number $k = 12$ cm^{-1} in the region $r/a \sim 0$–0.4) *versus* effective collisionality (at $r/a \sim 0$–0.1) in L-mode plasmas with pure-LHW heating and with combined heating of LHW and ECRH. The effective collisionality $\nu_{\rm eff}$ is defined as the electron–ion collision frequency normalized to the electron curvature drift frequency, and expressed as[38]

$$\nu_{\rm eff} = \nu_{\rm ei}/\omega_{\rm De} \sim 10^{-14} \cdot n_{\rm e} \cdot Z_{\rm eff} \cdot T_{\rm e}^{-2} \cdot R, \quad (2)$$

where $Z_{\rm eff}$ is the effective charge number and R is the major radius. The integrated power of turbulence can be obtained from the following equation:

$$S_{\rm k}(t) = \int_0^{\rm max} S(t,f)\,{\rm d}f, \quad (3)$$

where $S(t,f)$ refers to the spectrogram of microturbulence. As shown in Fig. 8, the measured $\tau_{\rm imp}$ values have a tendency of increase with the $\nu_{\rm eff}$ as shown by the dashed blue line. It is clearly shown that the $\tau_{\rm imp}$ and $\nu_{\rm eff}$ values are lower in the shots with combined heating of LHW and ECRH than that with pure-LHW heating.

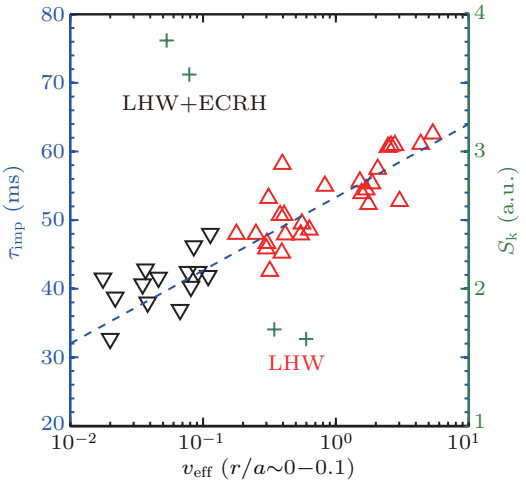


Fig. 8. Measured $\tau_{\rm imp}$ values (circles) and integrated power of turbulence $S_{\rm k}$, (green crosses) *versus* effective collisionality ($\nu_{\rm eff}$) at $r/a \sim 0$–0.1 in L-mode plasmas with pure-LHW heating (red) and with combined heating of LHW and ECRH (black).

In order to investigate the influence of the combined heating on core impurity confinement, two similar sawtooth-free L-mode discharges with different heating methods are chosen for comparison. The experimental conditions and plasma parameters of shots #59075 and #59093 are presented in Table 1, *e.g.*, $I_{\rm P} = 0.4$ MA, $\bar{n}_{\rm e} \sim 2.5 \times 10^{19}$ m^{-3}, $B_{\rm t} = 2.3$ T, and the same total heating power. Shot #59075 is heated by pure LHW with $P_{\rm LHW} = 1.9$ MW, while shot #59093 is heated by LHW with $P_{\rm LHW} = 1.6$ MW and ECRH with $P_{\rm ECRH} = 0.3$ MW. It is found that the combined heating of LHW and ECRH reduces the $\tau_{\rm imp}$ from ~ 62.78 ms to ~ 48.33 ms, and improves the energy confinement time $\tau_{\rm E}$ ($\tau_{\rm E} = W_{\rm MHD}/(P_{\rm total} - {\rm d}W_{\rm MHD}/{\rm d}t)$) from 36.8 ms to 49.8 ms. The reduced $\tau_{\rm imp}$ and improved $\tau_{\rm E}$ demonstrate an effective control of impurity and energy confinement by the combined heating of LHW and ECRH. With this combined heating, the $\beta_{\rm P}$ is improved from ~ 0.55 to ~ 0.9.

Table 1. Comparison between $\tau_{\rm imp}$ in LHW (#59075) and in LHW+ECRH (#59093) heated L-mode plasmas.

	#59075	#59093
Heating patterns	LHW (1.9 MW)	LHW+ECRH (1.6 MW+0.3 MW)
$I_{\rm p}$ (MA)	0.4	0.4
$\bar{n}_{\rm e}$ (10^{19} m^{-3})	2.5	2.5
$B_{\rm t}$ (T)	2.3	2.3
$W_{\rm MHD}$ (kJ)	52.6	76.2
$\beta_{\rm P}$	0.55	0.9
$\tau_{\rm E}$ (ms)	36.8	49.8
$\tau_{\rm imp}$ (ms)	62.78	48.33

The electron density and temperature profiles of the L-mode discharges with these two kinds of heating methods are shown in Fig. 9. The chosen shots have the parameters of $I_P = 0.45$ MA, $\bar{n}_e \sim 1.8 \times 10^{19}$ m^{-3}, and the same total heating power $P_{total} = 2.0$ MW. The red line indicates the discharge with the pure LHW heating ($P_{LHW} = 2.0$ MW), and the black line indicates the discharge with the combined heating of LHW and ECRH ($P_{LHW} = 1.5$ MW and $P_{ECRH} = 0.5$ MW). As shown in Fig. 9, in the case of combined heating of LHW and on-axis ECRH, a fairly peaked electron temperature profile and a relatively flat density profile in core plasma are achieved. The mechanism of τ_{imp} reduction has not been clarified yet. This intense central electron temperature ($T_e(0)$) would be responsible for the shorter τ_{imp} in the shots with combined heating described above. On the one hand, the pump-out effect of intense $T_e(0)$[39] can flatten main ion density gradient and thus reduce neoclassical convection for impurities.[4] On the other hand, higher $T_e(0)$ and lower central electron density can reduce the ν_{eff} in the core plasma, and thus yielding a low k electron mode such as trapped electron mode (TEM) turbulent transport dominated.[15] An enhanced microinstability at $k = 12$ cm^{-1} in the central region ($r/a \leq 0.4$) is observed by the tangential CO_2 laser collective scattering system[41] in the shots with combined heating of LHW and ECRH as shown by the green crosses in Fig. 8. The turbulent transport associated with these low k electron modes such as TEM can produce a decreased inward pinch and even an outward pinch of impurity,[42,43] yielding a shorter τ_{imp}. The TEM is often dominant in a low collisionality plasma which has been confirmed by gyrokinetic calculations in TCV.[44] In EAST, the TEM is also testified to be stronger than the electron temperature gradient (ETG) modes at $r/a \sim 0.4$ by the integrated modeling calculations in this combined heating case.[45]

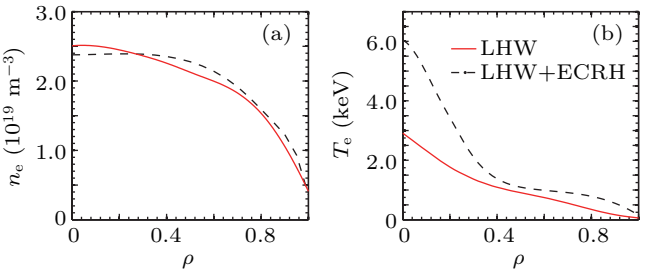


Fig. 9. (a) Electron density profiles and (b) temperature profiles of shots at $I_P = 0.45$ MA and $\bar{n}_e \sim 1.8 \times 10^{19}$ m^{-3} with the same total heating power, where solid red line denotes the shot with source power of $P_{LHW} = 2.0$ MW, dashed black line represents the shot with source power of $P_{LHW} = 1.5$ MW and $P_{ECRH} = 0.5$ MW, and ρ is the square root of normalized poloidal flux.

3.3. Impurity confinement in LHW and ECRH heated small ELMy H-mode plasmas

The analysis in sawtooth-free L-mode plasma shows that the core impurity confinement can be effectively reduced by combined heating of LHW and ECRH, which will be a good candidate heating method for the steady-state long-pulse and high-performance operation in EAST with tungsten divertor. In the 2017 EAST campaign, a long-pulse steady-state small ELMy H-mode with a duration of over 100 s and confinement factor $H_{98} > 1.1$ was achieved by using the pure RF heating (ICRF, LHW, and ECRH) with tungsten divertor.[46] It is also found that the preset long-pulse steady-state and high-performance discharges were always terminated by tungsten accumulation if the ECRH heating was turned off in advance.

The impurity confinement in H-mode plasmas heated by the combination of LHW heating and ECRH heating is explored on EAST, for the small-amplitude and high-frequency ELM regime ($f_{ELM} > 200$ Hz) often occurs in the high β_P discharges.[47] The comparisons among τ_{imp} and the β_N (normalized plasma thermal pressure) in L-mode, high-enhanced-recycling (HER) mode, and small ELMy H-mode are performed and the results are shown in Fig. 10. This figure shows $\tau_{imp} = 30$ ms–88 ms in L-mode discharges, $\tau_{imp} = 140$ ms–178 ms in HER H-mode discharges which operated with $P_{LHW} = 2$ MW–4 MW, and $\tau_{imp} = 40$ ms–80 ms in small ELMy H-mode discharges by using the combination of LHW heating and ECRH heating. Noticeably, the τ_{imp} in the small ELMy H-mode showing a level close to L-mode discharges is apparently shorter than that in HER H-mode discharges.[13,48,49] With the sufficient central heating and well controlled impurities[50] in this small ELMs regime, a higher $\beta_N \sim 1.7$ can be obtained.

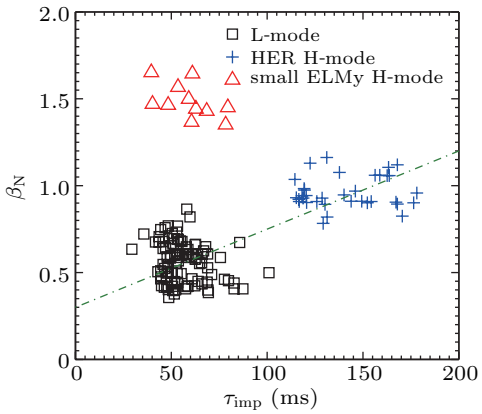


Fig. 10. β_N *versus* τ_{imp} in L-mode (black squares), HER H-mode (blue crosses), and small ELMy H-mode (red tringles).

Generally, in EAST routine discharges with this combined heating regime ($P_{LHW} > 1.7$ MW and $P_{ECRH} > 0.5$ MW), small ELMy H-mode with $f_{ELM} = 0.5$ kHz–1.4 kHz can be accessed. Shot #93624 is a typical discharge, which has the parameters of $I_P = 0.4$ MA, $\bar{n}_e \sim 3.9 \times 10^{19}$ m^{-3}, $B_t = 2.55$ T, source heating power $P_{LHW} = 1.9$ MW, and $P_{ECRH} = 0.5$ MW after $t = 2.92$ s, which are shown in Fig. 11. During this kind of combined heating phase, the edge coherent mode (ECM) is weakened, the $T_e(0)$ is about 3.2 keV, meanwhile a confinement factor $H_{98} \sim 1.3$ and $\beta_P \sim 1.35$ are achieved.

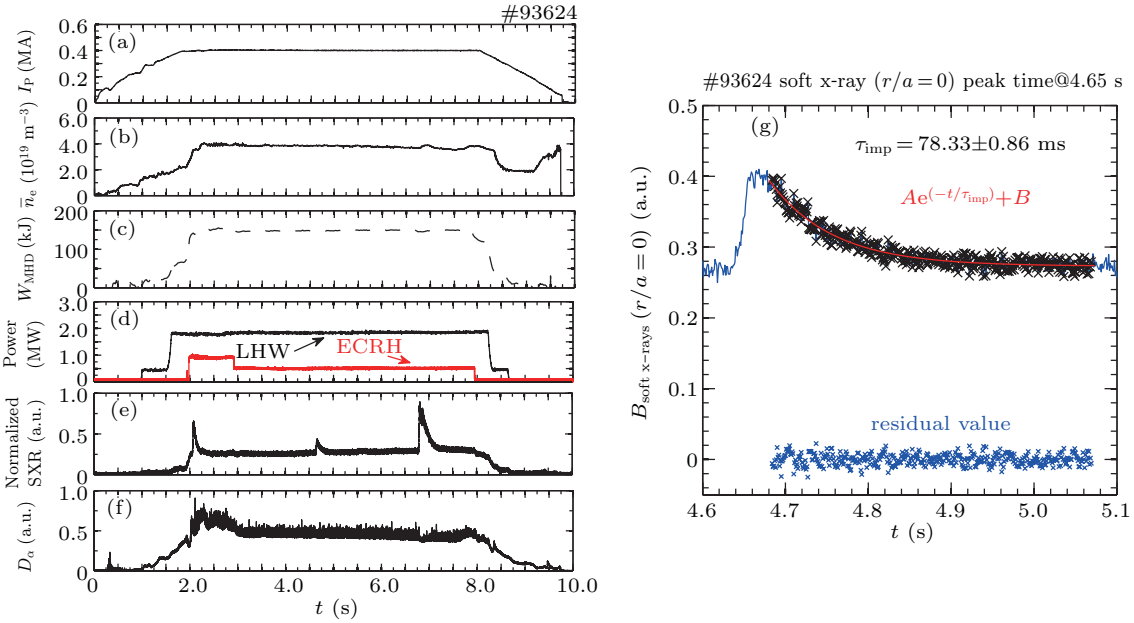


Fig. 11. Waveforms of shot #93624: (a) plasma current I_P, (b) line-averaged electron density $\bar{n}_e$, (c) stored energy W_{MHD}, (d) LHW and ECRH heating power P_{LHW} and P_{ECRH}, (e) normalized soft x-ray emission intensity from central LOS, (f) D_α intensity from upper divertor, and (g) impurity confinement time τ_{imp} during LHW+ECRH heating phase.

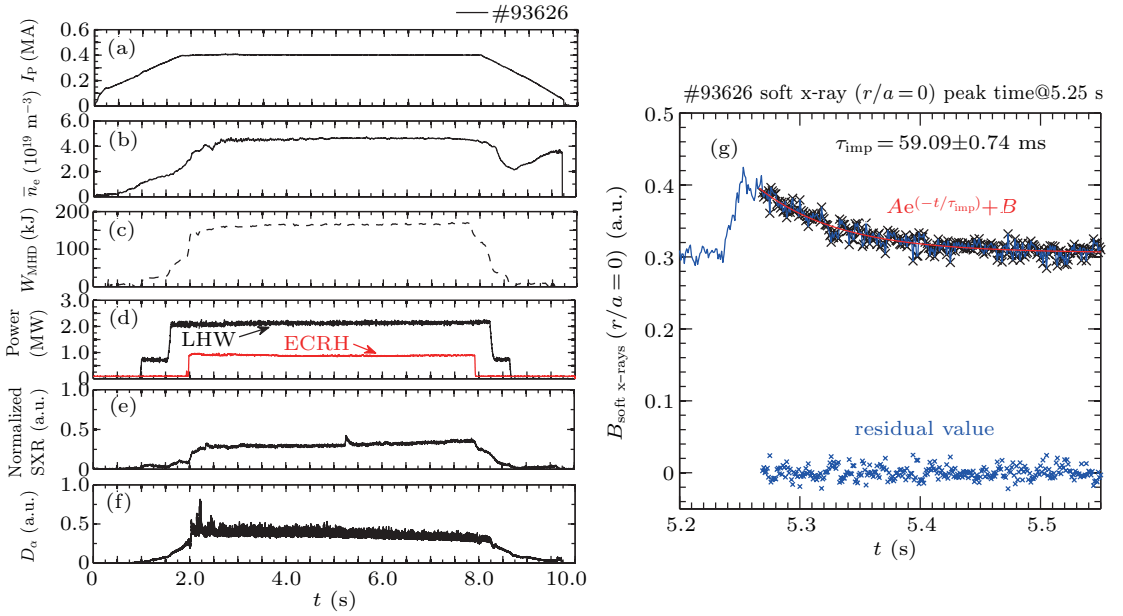


Fig. 12. Waveforms of shot #93626: (a) plasma current I_P, (b) line-averaged electron density $\bar{n}_e$, (c) stored energy W_{MHD}, (d) LHW and ECRH heating powers P_{LHW} and P_{ECRH}, (e) normalized soft x-ray emission intensity from central LOS, (f) D_α intensity from upper divertor, and (g) the impurity confinement time τ_{imp} during LHW+ECRH heating phase.

During the steady state phase, one spontaneous impurity Fe burst (without influence on ELM) at 4.65 s is observed and used to calculate the τ_{imp}. As shown in Fig. 11(g), the calculated τ_{imp} is about 76.33 ms. In this discharge, the ratio of τ_E ($\sim$ 86.13 ms) to τ_{imp} reaches up to $\sim$ 1.1, this ratio level is nearly twice that in HER H-mode regime heated by pure LHW.[13] The above analysis shows the combined heating of LHW and ECRH accompanied with small amplitude and high frequency ELMs has a great capacity for flushing out the impurities,[51] suggesting a good candidate regime for realizing the steady state and high performance operation of EAST 1000 s goal in future.

It should be pointed out that in this regime, τ_{imp} (τ_E/τ_{imp}) can be further reduced (increased) by improving the total power of this combined heating, such as in shot #93626. This shot has the following parameters: $I_P = 0.4$ MA, $\bar{n}_e \sim 4.5 \times 10^{19}$ m^{-3}, $B_t = 2.55$ T, and a higher source power of LHW and ECRH ($P_{LHW} = 2.2$ MW and $P_{ECRH} = 0.9$ MW) as shown in Fig. 12. The f_{ELM} in this shot is similar to that in #93624. The calculated τ_{imp} in this shot (Fe burst at 5.25 s) is reduced to 59.09 ms, and the τ_E/τ_{imp} is improved to $\sim$ 1.24 ($\tau_E \sim$ 73.3 ms). Comparing with the shot #93624, the reduc-

tion of impurity confinement and energy confinement are associated with the very centrally peaked electron temperature ($T_e(0) \sim 4.5$ keV). The higher $T_e(0)$ can result in the increasing of electron thermal diffusivity χ_e [15] and impurity diffusivity D_{imp}.[35] The increased τ_E/τ_{imp} indicates that the enhancement of the impurity particles' transport is more significant than that of the electron thermal transport by improving the total heating power in this regime.

Tungsten concentration ($C_W = n_w/n_e$, n_w and n_e are the tungsten ion density and electron density respectively, inside LCFS) is also investigated in this ELMy H-mode regime with LHW power scanning, such as in shot #88073. This shot has the parameters of $I_P = 0.4$ MA, $\bar{n}_e \sim 3.3 \times 10^{19}$ m^{-3}, $B_t = 2.55$ T, $P_{ECRH} = 0.7$ MW, and P_{LHW} is scanned from 2 MW to 3.5 MW from 2.5 s to 7.5 s as shown in Fig. 13. In this small ELMs regime, it is clearly seen that the C_W is well controlled at 10^{-5} level (C_W always exceeds 10^{-4} in type-I ELMy H-mode[52]) and can be further reduced from $\sim 5.0 \times 10^{-5}$ to $\sim 2.5 \times 10^{-5}$ with the decrease of ν_{eff}. As ν_{eff} is proportional to $T_e(0)^{-2} \cdot Z_{eff}$, the ν_{eff} is more sensitive to $T_e(0)$ than to Z_{eff}, which can be checked in Figs. 13(d) and 13(e). It is noted that the ν_{eff} just decreases slightly after 3.8 s where decreasing rate of the $T_e(0)$ becomes slow and Z_{eff} increases continuously. Two potential reasons of the slow change of $T_e(0)$ after 3.8 s are given in Ref. [53]: one is that the increase of Z_{eff} reduces the current drive efficiency, the other is that with P_{LHW} increasing, the parametric decay instability is enhanced, thus reducing the fraction of LHW power absorbed by plasma. Continuous growth of Z_{eff} during the LHW ramping-up phase is most likely caused by the impurity sputtering from the interactions between ELMs and surface or the 'hotspot' often occurring in the case of high P_{LHW}.[54] The increased C_W after 6.2 s is due to tungsten droplet events. Using this droplet event, the tungsten confinement time is also evaluated to be about 68.5 ms. The results imply that the combined heating of LHW and on-axis ECRH with sufficient high power injection can reduce the collisionality, and thus controlling high-Z impurities' accumulation.

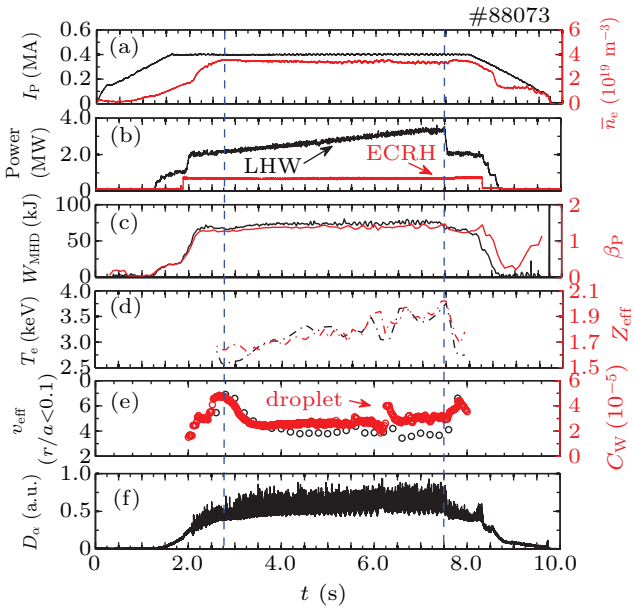


Fig. 13. Waveform of shot #88073: (a) plasma current I_P and line-averaged electron density $\bar{n}_e$, (b) LHW and ECRH heating power P_{LHW} and P_{ECRH}, (c) plasma stored energy W_{MHD} and normalized poloidal beta β_P, (d) central electron temperature $T_e(0)$ and effective charge number Z_{eff}, (e) effective collisionality ν_{eff} inside $r/a = 0.1$ and tungsten concentration C_W, and (f) D_α emission from upper divertor. The abrupt increase of tungsten concentration at 6.2 s is due to tungsten droplet.

The H_{98}, τ_{imp}, and the maximum duration values of L-mode, HER H-mode, and small ELMy H-mode plasma heated by RF heating are listed in Table 2. It is found that the small ELM regime has a higher H_{98}, a lower τ_{imp} and the longer pulse duration than other H-mode regimes on EAST, which shows that the small ELM regime will be more competitive in exploring long-pulse steady-state and high-performance operation in future tokamak devices with high-Z material PFCs like tungsten. More detailed analysis of the impurity and electron heat transport with small ELM regime is worth being performed, which can be helpful for further development on EAST.

Table 2. H_{98}, τ_{imp}, and the longest pulse duration in EAST typical several regimes.

	Heating patterns	H_{98}	τ_{imp} (ms)	Max. duration (s)
L-mode	Ohmic	0.5	42–88	–
L-mode	LHW/LHW+ECRH	0.6	30–60	411
HER H-mode	LHW+ECRH+ICRF	1.1	120–178	64.6
Small ELMy H-mode	LHW+ECRH+ICRF	1.3	40–80	14.6

4. Summary and discussion

Using the spontaneous transient perturbations of impurities, the core impurity confinement characteristics in sawtooth-free L- and small ELMy H-mode plasma heated jointly by LHW and ECRH on EAST are investigated experimentally. It has been verified that the combined heating regime can provide a sufficient central electron heating and lead to a reduced ν_{eff} in core plasma, which is beneficial to inhibiting the high-Z impurities' accumulation. In the L-mode plasma, τ_{imp} in shot with combined heating of LHW and ECRH is apparently lower than that in the shot with pure LHW heating, even if these shots have the same P_{total} and similar plasma parameters.

The dependence of τ_{imp} on the $\bar{n}_e$ and P_{total} in LHW+ECRH heated plasma is also investigated and compared with that in LHW-only heated plasma. In shots with the combined heating of LHW and ECRH, it is found that τ_{imp} is weakly dependent on $\bar{n}_e$, but strongly dependent on P_{total} dominated by LHW heating. Surely, the on-axis ECRH heating plays an essential role in this performance. With the help of the increased central electron temperature provided by the synergy between LHW and ECRH can foster more LHW power deposition near the plasma center. Thus, a peaked electron temperature profile can be achieved, and relevant turbulent transport such as TEM will be dominating in low ν_{eff} plasma and responsible for the enhanced transport observed in experiment. The results indicate that this combined heating method can avoid the serious impurity accumulation and is beneficial to β_P improvement.

Since high β_P regimes are favorable for the access to the small ELM regime, the impurity suppressing effect by this combined heating regime is also testified in the H-mode plasma. Comparing with HER H-mode regime, an L-mode level τ_{imp} and higher β_N are obtained in small ELM regime heated by this combined heating method. It also shows that the further increasing of the total power of LHW and ECRH is beneficial to τ_{imp} reduction and τ_E/τ_{imp} (>1) improvement. The LHW power scanning experiments verify that the tungsten ion concentration can decrease by reducing the ν_{eff}. The above results indicate that the lower ν_{eff} accompanied with small amplitude and high frequency ELM has a great capacity in flushing out the impurities from core plasma. Compared with other regimes, the small ELM regime heated by this combined heating scenario will be beneficial to the steady high-performance long-pulse operations in future devices with high-Z material (*e.g.*, tungsten) plasma-facing components.

References

[1] Isler R C 1984 *Nucl. Fusion* **24** 1599
[2] Isler R C, Roman W L and Hodge W L 1985 *Phys. Rev. Lett.* **55** 2413
[3] Philipps V 2011 *J. Nucl. Mater.* **415** S2
[4] Dux R, Neu R, Peeters A G, Pereverzev G, Mück A, Ryter F, Stober J and ASDEX Upgrade Team 2003 *Plasma Phys. Control. Fusion* **45** 1815
[5] Leigheb M, Romanelli M, Gabellieri L, Carraro L, Mattioli M, Mazzotta C, Puiatti M E, Lauro-Taroni L, Marinucci M, Nowak S, Panaccione L, Pericoli V, Smeulders P, Tudisco O, Sozzi C, Valisa M and the FTU team 2007 *Plasma Phys. Control. Fusion* **49** 1897
[6] Puiatti M E, Valisa M, Mattioli M, Bolzonella T, Bortolon A, Coffey I, Dux R, Hellermann M von, Monier-Garbet P, Nave M F F, Ongena J and contributors to the EFDA-JET Workprogramme 2003 *Plasma Phys. Control. Fusion* **45** 2011
[7] Cui Z Y, Zhang K, Morita S, Ji X Q, Ding X T, Xu Y, Sun P, Gao J M, Dong C F, Zheng D L, Li Y G, Jiang M, Li D, Zhong W L, Liu Yi, Dong Y B, Song S D, Yu L M, Shi Z B, Fu B Z, Lu P, Huang M, Yuan B S, Yang Q W and Duan X R 2018 *Nucl. Fusion* **58** 056012
[8] Odstrcil T, Howard N T, Sciortino F, Chrystal C, Holland C, Hollmann E, McKee G, Thome K E and Wilks T M 2020 *Phys. Plasma* **27** 082503
[9] Perry M E, Brooks N H, Content D A, Hulse R A, Ali Mahdavi M and Moos H W 1991 *Nucl. Fusion* **31** 1859
[10] Angioni C, Sertoli M, Bilato R, Bobkov V, Loarte A, Ochoukov R, Odstrcil T, Pütterich T, Stober J and The ASDEX Upgrade Team 2017 *Nucl. Fusion* **57** 056015
[11] Scavino E, Bakos J, Weisen H and TCV Team 2004 *Plasma Phys. Control. Fusion* **46** 857
[12] Parisot T, Guirlet R, Bourdelle C, Garbet X, Dubuit N, Imbeaux F and Thomas P R 2008 *Plasma Phys. Control. Fusion* **50** 055010
[13] Xu Z, Wu Z W, Zhang L, Gao W, Ye Y, Chen K Y, Yuan Y, Zhang W, Yang X D, Chen Y J, Zhang P F, Huang J, Wu C R, Morita S, Oishi T, Zhang J Z, Duan Y M, Zang Q, Ding S Y, Liu H Q, Chen J L, Hu L Q, Xu G S, Guo H Y and the EAST team 2018 *Nucl. Fusion* **58** 016001
[14] Zhang L, Morita S. Xu Z, Zhang P F, Zang Q, Duan Y M, Liu H Q, Zhao H L, Ding F, Oishi T, Gao W, Huang J, Yang X D, Chen Y J, Wu Z W, Xu P, Ding B J, Hu C D, Gong X Z, Hu L Q and EAST team 2017 *Nucl. Mater. Energy* **12** 774
[15] Du H F, Ding S Y, Chen J L, Wang Y F, Lian H, Xu G S, Zhai X M, Liu H Q, Zang Q, Lyu B, Duan Y M, Qian J P and Gong X Z 2018 *Nucl. Fusion* **58** 066011
[16] Yang Y L, Xiang N and Hu Y M 2017 *Phys. Plasma* **24** 082503
[17] Giruzzi G, Artaud J F, Dumont R J, Imbeaux F, Bibet P, Berger-By G, Bouquey F, Clary J, Darbos C, Ekedahl A, Hoang G T, Lennholm M, Maget P, Magne R, Ségui J L, Bruschi A and Granucci G 2004 *Phys. Rev. Lett.* **93** 255002
[18] Yuan Y, Hu L Q, Wang X G, Wang X J, Xu H D, Luo Z P, Chen K Y, Lin S Y, Duan Y M, Chang P X, Zhao H L, He K Y and Liang Y F 2016 *Phys. Plasma* **23** 062503
[19] Liu Z X, Gao X, Jie Y X, Ding B J and Yang Y 2012 *Plasma Sci. Technol.* **14** 278
[20] Nave M F F, Rapp J, Bolzonella T, Dux R, Mantsinen M J, Budny R, Dumortier P, von Hellermann M, Jachmich S, Koslowshi H R, Maddison G, Messiaen A, Monier-Garbet P, Ongena J, Puiatti M E, Strachan J, Telesca G, Unterberg B, Valisa M, de Vries P and contributors to the JET-EFDA Workprogramme 2003 *Nucl. Fusion* **43** 1204
[21] Wan Y X, Li J G, Weng P D and EAST team 2006 *Plasma Sci. Technol.* **8** 253
[22] Zhao L M, Shan J F, Liu F K, Jia H, Wang M, Liu L, Wang X J, Xu H D and LHCD team 2010 *Plasma Sci. Technol.* **12** 118
[23] Liu F K, Ding B J, Li J G, Shan J F, Wang M, Liu L, Zhao L M, Li M H, Li Y C, Yang Y, Wu Z G, Feng J Q, Hu H C, Jia H, Huang Y Y, Wei W, Cheng M, Xu L, Zang Q, Lyu B, Lin S Y, Duan Y M, Wu J H, Peysson Y, Decker J, Hillariret J, Ekedahi A, Luo Z P, Qian J P, Shen B, Gong X Z, Hu L Q and the EAST team 2015 *Nucl. Fusion* **55** 123022
[24] Zhao Y P, Zhang X J, Mao Y Z, Yuan S, Xue D Y, Deng X, Wang L, Ju S Q, Cheng Y, Qin C M, Chen G, Lin Y, Li J G, Wan B N, Song Y T, Braun F, Kumazawa R and Wukitch S 2014 *Fusion Eng. Des.* **89** 2642
[25] Wang X J, Liu F K, Shan J F, Xu H D, Wu D J, Li B, Wei W, Zhang J, Huang Y Y, Tang Y Y, Xu W Y, Hu H C, Wang J, Xu L, Zhang Y Y and Feng J Q 2015 *Fusion Eng. Des.* **96** 181
[26] Chen K Y, Xu L Q, Hu L Q, Duan Y M, Li X Q, Yuan Y, Mao S T, Sheng X L and Zhao J L 2016 *Rev. Sci. Instrum.* **87** 063504
[27] Zhang L, Morita S, Xu Z, Wu Z W, Zhang P F, Wu C R, Gao W, Oishi T, Goto M, Shen Y C, Chen Y J, Liu X, Wang Y M, Dong C F, Zhang H M, Huang X L, Gong X Z, Hu L Q, Chen J L, Zhang X D, Wan B N and Li J G 2015 *Rev. Sci. Instrum.* **86** 123509
[28] Seguin F H, Petrasso R and Marmar E S 1983 *Phys. Rev. Lett.* **51** 455
[29] Moret J M and Tore Supra 1992 *Nucl. Fusion* **32** 1241
[30] Rice J E, Reinke M L, Gao C, Howard N T, Chilenski M A, Delgado-Aparicio L, Granetz R S, Greenward M J, Hubbard A E, Hughes J W, Lrby J H, Lin Y, Marmar E S, Mumgaard R T, Scott S D, Terry J L, Walk J R, White A E, Whyte D G, Wolfe S M and Wukitch S J 2015 *Nucl. Fusion* **55** 033014
[31] Scavino E, Bakos J S, Dux R, Weisen H and TCV team 2003 *Plasma Phys. Control. Fusion* **45** 1961
[32] Mattioli M, Giannella R, Myrnas R, Demichelis C, Denne-Hinnov B, Dudok De Wit T and Magyar G 1995 *Nucl. Fusion* **35** 1115
[33] Leung W K, Rowan W L, Wiley J C, Bravenec R V, Gentle K W, Hodge W L, Patterson D M, Philliphs P E, Price T R and Richards B 1986 *Plasma Phys. Control. Fusion* **28** 1753
[34] Cesario R, Amicucci L, Cardinali A, Castaldo C, Marinucci M, Napoli F, Paoletti F, De Arcangelis D, Ferrari M, Galli A, Gallo G, Pullara E, Schettini G and Tuccillo A A 2014 *Nucl. Fusion* **54** 043002
[35] Dux R and Peeters A G 2000 *Nucl. Fusion* **40** 1721
[36] Dumont R J and Giruzzi G 2004 *Phys. Plasma* **11** 3449

[37] Wan B N, Liang Y F, Gong X Z, Xiang N, Xu G S, Sun Y W, Wang L, Qian J P, Liu H Q, Zeng L, Zhang L, Zhang X J, Ding B J, Zang Q, Lyu B, Garofalo A M, Ekedahi A, Li M H, Ding F, Ding S Y, Du H F, Kong D F, Yu Y, Yang Y, Luo Z P, Huang J, Zhang T, Zhang Y, Li G Q, Xia T Y, the EAST team and Collaborators 2019 *Nucl. Fusion* **59** 112003

[38] Puiatti M E, Valisa M, Angioni C, Garzotti L, Mantica P, Mattiolo M, Carraro L, Coffey I, Sozzi C and JET-EFDA contributors 2006 *Phys. Plasma* **13** 042501

[39] Andreev V F, Borschegovskij A A, Chistyakov V V, Dnestrovskij Y N, Gorbunov E P, Kasyanova N V, Lysenko S E, Melnikov A V, Myalton T B, Roy I N, Sergeev D S and Zenin V N 2016 *Plasma Phys. Control. Fusion* **58** 055008

[40] Takenaga H, Higashijima S, Oyama N, Bruskin L G, Koide Y, Ide S, Shirai H, Sakamoto Y, Suzuki T, Hill K W, Rewoldt G, Kramer G J, Nazikian R, Takizuka T, Fujita T, Sakasa A, Kamada Y, Kubo H and the JT-60 Team 2003 *Nucl. Fusion* **43** 1235

[41] Cao G M, Li Y D, Li Q, Zhang X D, Sun P J, Wu G J, Hu L Q and the EAST team 2015 *Phys. Scr.* **90** 025603

[42] Villegas D, Guirlet R, Bourdelle C, Hoang G T, Garbet X and Sabot R 2010 *Phys. Rev. Lett.* **105** 035002

[43] Shen Y C, Lyu B, Zhang H M, Li Y Y, Fu J, Vogel G, Wang X J, Xu H D, Wu D J, Zang Q, Liu H Q, Liu F K, Wan B N and Ye M Y 2019 *Phys. Plasma* **26** 032507

[44] Marinoni A, Brunner S, Camenen Y, Coda S, Graves J P, Lapillonne X, Pochelon A, Sauter O and Villard L 2009 *Plasma Phys. Control. Fusion* **51** 055016

[45] Huang Y H, *et al.,* 2020 *Nucl. Fusion* (under review)

[46] Gong X, Garofalo A M, Huang J, Qian J, Holcomb C T, Ekedah A, Maingi R, Li E, Zeng L, Zhang B, Chen J, Wu M, Du H, Li M, Zhu X, Sun Y, Xu G, Zang Q, Wang L, Zhang L, Liu H, Lyu B, Sun P, Ding S, Zhang X, Liu F, Zhao Y, Xiao B, Hu J, Hu C, Hu L, Li J, Wan B and the EAST team 2019 *Nucl. Fusion* **59** 086030

[47] Xu G S, Yang Q Q, Yan N, Wang Y F, Xu X Q, Guo H Y, Maingi R, Wang L, Qian J P, Gong X Z, Chan V S, Zhang T, Zang Q, Li Y Y, Zhang L, Hu G H and Wan B N 2019 *Phys. Rev. Lett.* **122** 255001

[48] Wang H Q, Xu G S, Wan B N, Ding S Y, Guo H Y, Shao L M, Liu S C, Xu X Q, Wang E, Yan N, Naulin V, Nielsen A H, Juul Rasmussen J, Candy J, Bravenes R, Sun Y W, Shi T H, Liang Y F, Chen R, Zhang W, Wang L, Chen L, Zhao N, Li Y L, LIU Y L, Hu G H and Gong X Z 2014 *Phys. Rev. Lett.* **112** 185004

[49] Wang H Q, Xu G S, Guo H Y, Wan B N, Yan N, Ding S Y, Chen R, Zhang W, Wang L, Liu S C, Shao L M, Chen L, Liu Y L, Li Y L, Hu G H and Zhao N 2014 *Nucl. Fusion* **54** 043014

[50] Gao X, Yang Y, Zhang T, Liu H Q, Li G Q, Ming T F, Liu Z X, Wang Y M, Zeng L, Han X, Liu Y K, Wu M Q, Qu H, Shen B, Zang Q, Yu Y W, Kong D F, Gao W, Zhang L, Cai H S, Wu X M, Hanada K, Zhong F B, Liang Y F, Hu C D, Liu F K, Gong X Z, Xiao B J, Wan B N, Zhang X D, Li J G and the EAST team 2017 *Nucl. Fusion* **57** 056021

[51] Pütterich T, Dux R, Janzer M A, McDermott R M and ASDEX Upgrade team 2011 *J. Nucl. Mater.* **415** S334

[52] Xu Z, *et al.,* 2020 *Plasma Phys. Control. Fusion* (under review)

[53] Li M H, Ding B J, Liu F K, Shan J F, Wang M, Xu H D, Cesario R, Napoli F, Castaldo C, Cardinali A, Liu L, Zhao L M, Hu H C, Zhang X J, Li Y C, Wu Z G, Ma W D, Goniche M, Peysson Y, Ekedahl A, Zhang L, Lin S Y, Qian J P, Chen Y J, Yang Y, Feng J Q, Jia H, Wang Y F, Wu C B and the EAST team 2019 *Plasma Phys. Control. Fusion* **61** 065005

[54] Li Y L, Xu G S, Wu Z W, Zhang B, Zhang L, Yang X D, Chen M W, Zhang T, Liu H Q, Wan B N, Gong X Z, Goniche M, Ekedahi A, Warrier M, Xiao C, Gao W, Ou J, Cao L, Liu C L, Wang M, Li M H, Li Y C, Xu Q, Liang Y F, Wang L, Sun Z, Xu J C, Feng W, Yan N, Chen R and EAST team 2018 *Phys. Plasma* **25** 082503